NAD kinase controls antibiotic susceptibility and pathogenic potential in *Staphylococcus aureus*

Clarisse Leseigneur[1,2], Laurent Boucontet[3,4], Olivier Gorgette[5], Catherine Thouvenot[5], Emma Colucci-Guyon[3,4], Olivier Dussurget[1,2]*

[1]Unité de Recherche *Yersinia*, Institut Pasteur, Paris, France; [2]Université de Paris, Paris, France; [3]Unité Macrophages et Développement de l'Immunité, Institut Pasteur, Paris, France; [4]CNRS UMR 3738, Paris, France; [5]Unité Technologie et Service Bioimagerie Ultrastructurale, Institut Pasteur, Paris, France.

*For correspondence: olivier.dussurget@pasteur.fr

14 # Abstract

15

16 Nicotinamide adenine dinucleotide phosphate (NADPH) is the primary electron donor for
17 reductive reactions that are essential for the biosynthesis of major cell components in all
18 organisms. Nicotinamide adenine dinucleotide kinase (NADK) is the only enzyme that
19 catalyzes synthesis of NADP(H) from NAD(H). While the enzymatic properties and
20 physiological functions of NADK have been thoroughly studied, the role of NADK in
21 bacterial pathogenesis remains unknown. Here, we used CRISPR interference to knockdown
22 NADK gene expression in order to address the role of NADK in *Staphylococcus aureus*
23 pathogenic potential. We find that NADK protects bacteria from antimicrobial defense
24 mechanisms encountered in the host during infection such as oxidative and envelope stresses.
25 Furthermore, we show that antioxidant properties of NADK promote *S. aureus* survival in
26 infected macrophages. Remarkably, NADK inhibition drastically decreases mortality of
27 zebrafish infected with *S. aureus*. These findings support a key role for NADK in bacteria
28 interactions with innate immune cells and during infection. Last, we reveal that decreasing
29 NADK expression increases *S. aureus* susceptibility to antibiotics, opening the way to
30 development of synergistic treatments based on NADK inhibitors and current antibiotics.

31

32

33

Introduction

Nicotinamide adenine dinucleotide (NAD^+), its phosphorylated form ($NADP^+$) and their reduced equivalents (NADH and NADPH) are essential cofactors shared by all living organisms. While NAD^+ and NADH are important for cellular energy metabolism, inflammation and senescence (Chini et al., 2021; Covarrubias et al., 2021), $NADP^+$ and NADPH are key cofactors in central metabolism, being involved in tricarboxylic acid (TCA) cycle, pentose phosphate pathway as well as *de novo* synthesis of fatty acids, cholesterol, amino acids and nucleotides (Chandel, 2021). NADPH also provides the reducing power necessary for the restoration of antioxidative defense systems of the cell (Chandel, 2021). Like NAD(H), growing evidence suggests that NADP(H) has a broader role. In particular, the $NADP^+$ derivative nicotinic acid adenine dinucleotide phosphate (NAADP), which is the major intracellular calcium mobilizing molecule, links NADP(H) metabolism with calcium homeostasis and signaling, development and differentiation (Galione and Chuang, 2020).

Whereas there are two known multi-step pathways for NAD^+ biosynthesis, a single enzyme is responsible for the phosphorylation of NAD^+/NADH into $NADP^+$/NADPH: the NAD kinase (NADK) (McGuinness and Butler, 1985; Chini et al., 2021). NADK activity was first reported in the late 30's (Vestin, 1937; Von Euler and Adler, 1938), and the enzyme was purified from yeast by Kornberg in 1950 (Kornberg, 1950). It is only in 2000 that the genes encoding NADK were identified in *Micrococcus flavus* and *Mycobacterium tuberculosis* (Kawai et al., 2000). Since then, NADK genes have been identified in all living organisms, except the intracellular parasitic bacteria *Chlamydia* spp. on the basis of genome annotation (Grose et al., 2006; Fisher et al. 2013). Given the vital role of NADPH, notably during oxidative stress, NADK genes have been shown to be essential for growth of several bacteria, such as *Mycobacterium tuberculosis* (Sassetti et al., 2003), *Bacillus subtilis* (Kobayashi et al., 2003), *Salmonella enterica* (Grose et al., 2006) and *Staphylococcus aureus* (Chaudhuri et al.,

2009; Gelin et al., 2020). NADKs essentiality may account for the poor characterization of their role in prokaryotes. In contrast, NADKs have been extensively studied in plants (Li et al., 2018), especially in *Arabidopsis thaliana* which possesses three NADK encoding genes (Chai et al., 2006; Turner et al., 2004). NADK has a key role in photosynthesis, plant cell metabolism, intracellular redox balance (Li, 2018), and response to stresses as shown during exposure to aluminum in wheat (Ślaski, 1995), upon cold-shock in green bean leaves (Ruiz et al., 2002), upon treatment with NaCl, ionizing radiations or oxidative stress in *Arabidopsis thaliana* (Chai et al., 2006; Berrin et al., 2005).

In plants, NADKs are mainly regulated by calcium and calmodulin (Tai et al., 2019). In fact, NADK from peas extract has been historically used as a tool to examine calmodulin activity in proteins (Muto and Miyachi, 1977). In higher plants, activation of NADK was shown to be dependent on Ca^{2+}-dependent calmodulin complex formation and was inhibited by calcium chelation using EGTA (Jarrett et al., 1980). Some NADKs are regulated by direct interactions with Ca^{2+}-dependent calmodulins through their calmodulin-binding domains (Turner et al., 2004). Other NADKs have been proposed to be indirectly regulated through a Ca^{2+}/calmodulin-mediated kinase cascade (Love et al., 2015) and some NADK isoforms are calmodulin independent (Simon et al., 1982). In contrast, in prokaryotes allosteric regulation of NADK activity by NADPH or NADH is the only mechanism identified so far (Grose et al., 2006).

The importance of microbial metabolic adaptation during infection (Eisenreich et al., 2010; Richardson, 2019; Teoh et al., 2021) and the unknown contribution of NADK to bacterial pathogenesis prompted us to investigate the role of NADK in *Staphylococcus aureus*. While being carried as a commensal by around one third of the human population, *S. aureus* is a leading cause of infectious diseases, ranging from mild skin and soft tissue infections to life-threatening endocarditis and bacteremia (Turner et al., 2019). Worryingly, *S.*

aureus can develop resistance to virtually all antibiotic classes available (Vestergaard et al., 2019), limiting dramatically therapeutic options for some patients. Therefore, WHO included *S. aureus* in the list of high priority pathogens to promote research and development of new antibiotics and emphasized the need for innovation and diversification in the choice of targets (https://www.who.int/news/item/27-02-2017-who-publishes-list-of-bacteria-for-which-new-antibiotics-are-urgently-needed).

In this study, we used a genetic approach to modulate NADK activity and study *S. aureus* behavior in response to stresses mimicking those encountered during infection and antibacterial treatment. We show that exposures to oxidative, envelope or antibiotic-mediated stresses significantly decrease bacterial survival upon inhibition of NADK activity. Importantly, we demonstrate that inhibition of NADK leads to a dramatic decrease of *S. aureus* survival in a macrophage infection model, highlighting its role during interactions with immune cells. Finally, we establish the first link between NADK activity and *S. aureus* pathogenic potential, as NADK inhibition led to an increased survival of the host in a zebrafish infection model.

Results

S. aureus ppnK gene encoding NADK is part of the *relQ* operon

As most prokaryotes, *S. aureus* possesses a single NADK encoded by the highly conserved *ppnK* gene. To investigate expression of the *ppnK* genomic locus, we carried out RT-PCR on RNA purified from *S. aureus* Xen36 strain during exponential growth in BHI broth at 37°C. Cotranscript analysis revealed that *ppnK* belongs to the *relQ* operon (Figure 1, Figure supplement 1). The *relQ* gene is one of the three genes responsible for synthesis of the (p)ppGpp alarmones and synthesizes also the third alarmone pGpp. In addition the operon contains genes encoding a small hypothetical protein (00941), a pseudouridine synthase (00944), a putative magnesium transporter (00945) and a Na^+/H^+ antiporter-like protein (00946). Remarkably, synteny analysis showed that three genes of the *S. aureus relQ* operon, *i.e. relQ*, *ppnK* and *00944*, are conserved among *Bacilli* (Figure 1). This confirmed the importance of these genes and raised the possibility of a functional connection, in particular in adaptation to stress and pathogenesis.

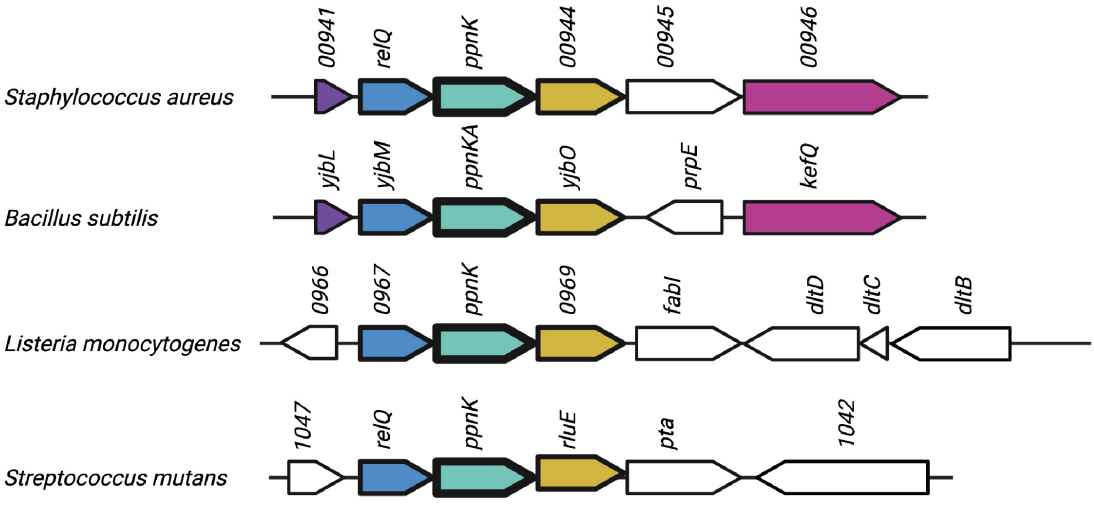

Figure 1. The *ppnK* genomic locus is conserved in *Bacilli*. Comparative analysis of the *ppnK* genomic locus of *S. aureus* NCTC8325, *Bacillus subtilis* 168, *Listeria monocytogenes* EGDe and *Streptococcus mutans* UA159 was performed using SyntTax. Arrows of the same color represent orthologs.

NADK protects *S. aureus* from hydrogen peroxide toxicity

To investigate the role of NADK in *S. aureus* stress response and pathogenesis, we took a genetic approach to modulate the expression of *ppnK*. We used the *S. aureus* Xen36/NADK sgRNA strain in which the levels of *ppnK* expression were decreased by CRISPR-based interference (Gelin et al., 2020). Knockdown of NADK expression in this strain was verified by RT-PCR, immunoblotting and aerobic growth in BHI at 37°C (Figure supplement 2). An important host defense encountered by bacteria during infection is the production of toxic levels of reactive oxygen species (ROS) (Avican et al., 2021; Fang et al., 2016). We therefore compared growth of the *S. aureus* strain containing the empty vector to that of the NADK knockdown strain, upon exposure to increasing concentrations of hydrogen peroxide (H_2O_2). While the Xen36/pSD1 strain resisted to high doses of H_2O_2, the Xen36/NADK sgRNA strain showed increasing growth deficiency when exposed to H_2O_2 concentrations ranging from 50 to 500 µM H_2O_2 (Figure 2A). Expectedly, treatment of the Xen36/pSD1 strain with catalase alone or catalase and H_2O_2 did not affect growth (Figure 2B). In contrast, addition of catalase, which catalyzes hydrogen peroxide dismutation into water and oxygen, rescued the growth defect of the Xen36/NADK sgRNA strain upon H_2O_2 treatment (Figure 2B). Taken together, our results show that NADK protects *S. aureus* from toxic effects of a reactive oxygen species involved in host defense.

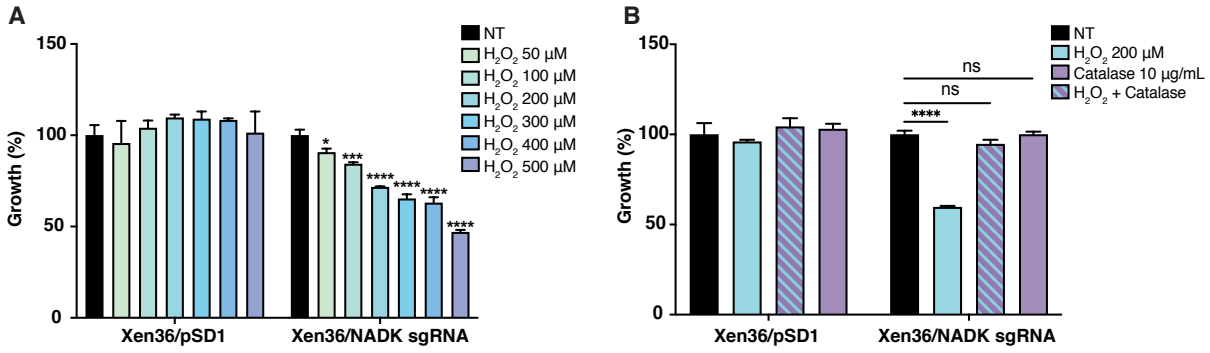

Figure 2 NADK protects *S. aureus* from hydrogen peroxide toxicity. Bacterial growth was monitored at OD_{600nm} in BHI broth at 37°C. (A) Percentage of growth of the *S. aureus* strain containing the empty vector (Xen36/pSD1) and the *ppnK* knock-down strain (Xen36/NADK sgRNA) exposed for 6 hours to increasing concentrations of H_2O_2 relative to the untreated

condition (NT). (B) Percentage of growth of the *S. aureus* strain containing the empty vector (Xen36/pSD1) and the *ppnK* knockdown strain (Xen36/NADK sgRNA) exposed for 6 hours to H_2O_2 and catalase alone or in combination, relative to the untreated condition (NT). Data shown are representative of three independent experiments. Bars indicate the standard error of the means of biological replicates (n=3). Comparison of data was performed using one-way analysis of variance (ns: nonsignificant, *p<0.05, ***p<0.001, ****p<0.0001).

NADK protects *S. aureus* from envelope stress

Within the infected host, bacteria have to cope with multiple sources of envelope stress, such as bile salts, cationic antimicrobial peptides and osmotic stress (Avican et al., 2021; Fang et al., 2016). We therefore investigated the effects of NADK knockdown on *S. aureus* sensitivity to envelope stress. First we treated Xen36/pSD1 and Xen36/NADK sgRNA strains with triclosan, a membranotropic antibacterial agent and an inhibitor of FabI, an enoyl-ACP reductase implicated in the last step of bacterial fatty acid elongation (Guillén et al., 2004; Lu and Tonge, 2008). Xen36/NADK sgRNA displayed a higher susceptibility to 0.5 nM triclosan treatment compared to Xen36/pSD1 (Figure 3A). At nanomolar concentration and above, triclosan inhibited growth of both strains. Unexpectedly, catalase treatment rescued the growth defect of the *ppnK* knockdown strain upon exposure to 0.75 nM triclosan, suggesting a contribution of ROS in the antibacterial effect (Figure 3B). Next, we investigate the role of NADK in response to osmotic stress upon addition of NaCl to the broth. Xen36/NADK sgRNA was more sensitive to NaCl treatment than the Xen36/pSD1 strain at concentrations of 4% and above (Figure 3C). In contrast to triclosan, catalase treatment failed to rescue bacterial survival at 4% NaCl (Figure 3D), suggesting an H_2O_2-independent antibacterial effect in our experimental conditions. Interestingly, using electron microscopy, we observed that NADK inhibition led to membrane permeabilization and cytoplasmic content leakage (Figure supplement 2D). Together, these results show that NADK contributes to *S. aureus* envelope integrity upon stress.

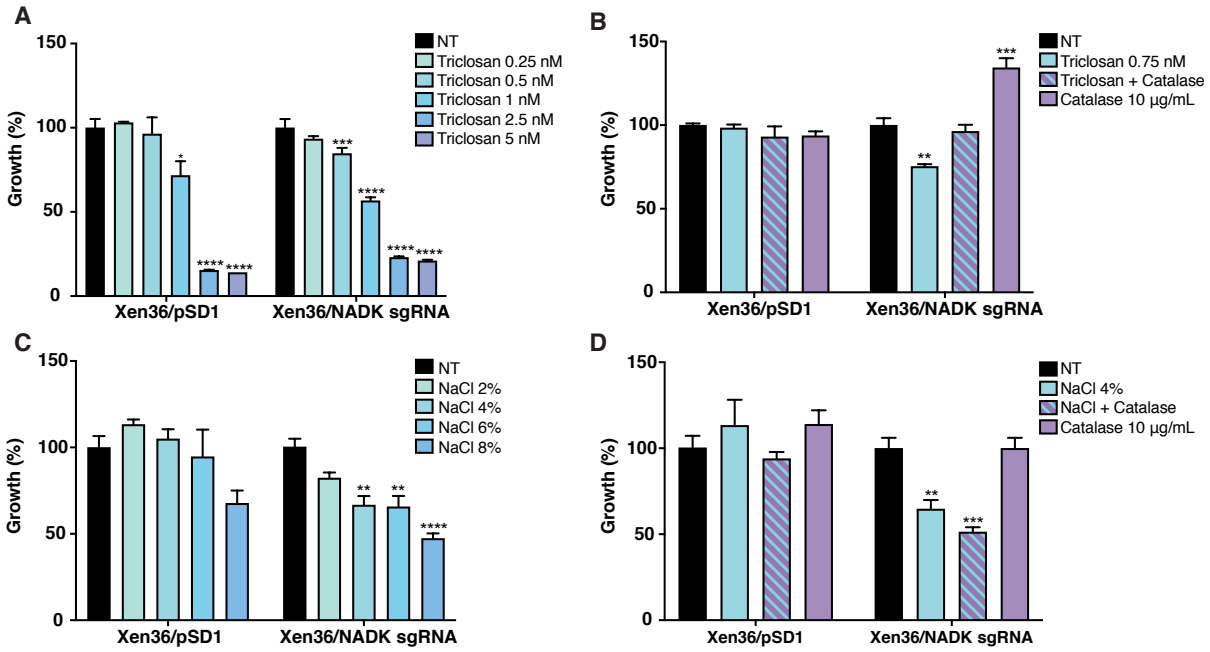

Figure 3 NADK protects *S. aureus* from envelope stress. Bacterial growth was monitored at OD_{600nm} in BHI broth at 37°C. (A) Percentage of growth of the *S. aureus* strain containing the empty vector (Xen36/pSD1) and the *ppnK* knock-down strain (Xen36/NADK sgRNA) exposed for 6 hours to increasing concentrations of triclosan relative to the untreated condition (NT). (B) Percentage of growth of the *S. aureus* strain containing the empty vector (Xen36/pSD1) and the *ppnK* knockdown strain (Xen36/NADK sgRNA) exposed for 6 hours to triclosan and catalase alone or in combination, relative to the untreated condition (NT). (C) Percentage of growth of the *S. aureus* strain containing the empty vector (Xen36/pSD1) and the *ppnK* knockdown strain (Xen36/NADK sgRNA) exposed for 6 hours to increasing concentrations of NaCl relative to the untreated condition (NT). (D) Percentage of growth of the *S. aureus* strain containing the empty vector (Xen36/pSD1) and the *ppnK* knockdown strain (Xen36/NADK sgRNA) exposed for 6 hours to NaCl and catalase alone or in combination, relative to the untreated condition (NT). Data shown are representative of three independent experiments. Bars indicate the standard error of the means of biological replicates (n=3). Comparison of data was performed using one-way analysis of variance (ns: nonsignificant, *p<0.05, **p<0.01, ***p<0.001, ****p<0.0001).

NADK controls antibiotic susceptibility

It has been proposed that all bactericidal antibiotics kill bacteria through ROS production. Although it is a controversial issue, evidences support that some antibiotics such as aminoglycosides, fluoroquinolones and β-lactam antibiotics might activate the TCA cycle, leading to hyperactivation of the electron transport chain and superoxide radicals formation (Van Acker and Coenye, 2017; Baquero and Levin, 2021). In addition, several antibiotic

187 classes target the bacterial envelope (Baquero and Levin, 2021). As NADK protects *S. aureus*
188 from oxidative stress (Figure 2) and envelope stress (Figure 3), we wondered if *ppnK*
189 knockdown might impact bacterial survival under antibiotic-induced stress. To test this
190 hypothesis, we treated Xen36/pSD1 with subinhibitory concentrations of antibiotics of several
191 classes and compared its growth to that of the Xen36/NADK sgRNA strain. We first used
192 polymyxin B, an amphipatic cyclic lipopeptide disrupting bacterial membranes. As expected,
193 a concentration of polymyxin B as high as 40 μg/mL did not inhibit growth of the
194 Xen36/pSD1 strain (Figure 4A), *S. aureus* being notoriously resistant to polymyxins
195 (Vestergaard et al., 2017). In contrast, the Xen36/NADK sgRNA was susceptible to
196 polymyxin B in a ROS-dependent manner (Figure 4A). We then tested the effect of NADK
197 know-down on sensitivity to all the other major classes of antibiotics. Strikingly, the
198 Xen36/NADK sgRNA strain was susceptible to levofloxacin, a DNA gyrase and
199 topoisomerase IV inhibitor (Figure 4B), kanamycin, a protein synthesis inhibitor (Figure 4C)
200 and rifampicin, an RNA polymerase inhibitor (Figure 4D). Similarly to polymyxin B,
201 treatment with catalase alleviated toxicity of these three antibiotics (Figures 4A-D). The
202 knockdown of *ppnK* also led to decreased bacterial growth in the presence of vancomycin,
203 which inhibits peptidoglycan biosynthesis. However, catalase was unable to restore growth to
204 the level of non-treated bacteria, indicating that the growth defect was not due to ROS
205 production. Together, these results show that NADK activity controls antibiotics
206 susceptibility in ROS-dependent and ROS-independent manner.
207
208
209

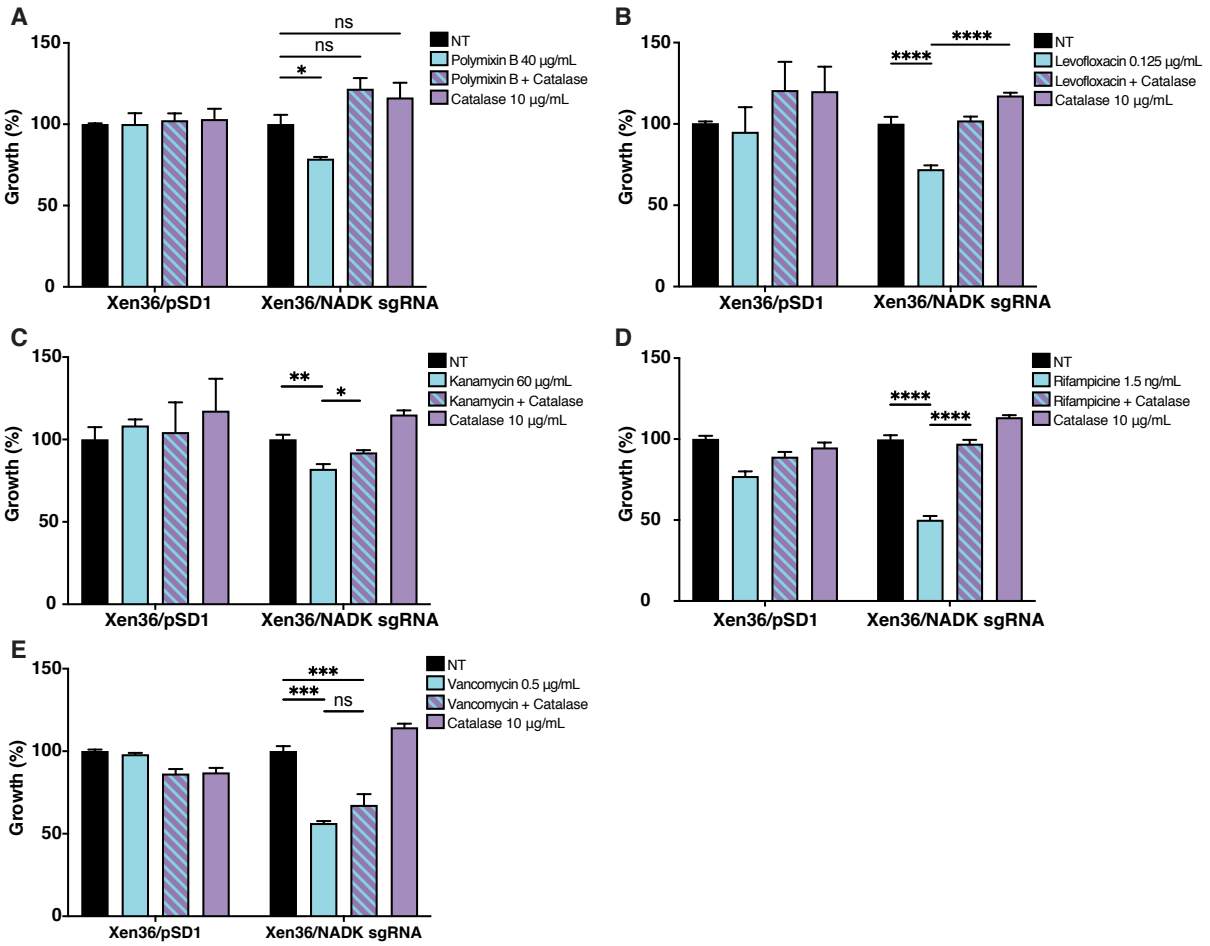

Figure 4 NADK controls antibiotic susceptibility. Bacterial growth was monitored at OD_{600nm} in BHI broth at 37°C. (A-E) Percentage of growth of the *S. aureus* strain containing the empty vector (Xen36/pSD1) and the *ppnK* knock-down strain (Xen36/NADK sgRNA) exposed to polymyxin B (A), levofloxacin (B), kanamycin (C), rifampicin (D), vancomycin (E) with and without catalase for 6 hours relative to the untreated condition (NT). Data shown are representative of three independent experiments. Bars indicate the standard error of the means of biological replicates (=3). Comparison of data was performed using one-way analysis of variance (ns: nonsignificant, *p<0.05, **p<0.01, ***p<0.001, ****p<0.0001).

NADK promotes *S. aureus* survival in macrophages

Since ROS production is a major antibacterial mechanism of key immune cells such as phagocytes, we next investigated if *ppnK* knockdown might impair *S. aureus* survival during macrophages infection. Murine RAW264.7 macrophages were infected with Xen36/pSD1 or Xen36/NADK sgRNA strains. Bacterial enumerations were performed at time zero and 1, 2, 4 and 6 hours post infection. No significant difference in phagocytosis of the two strains could be observed, nor at early time of infection (Figure 5A). In contrast, after 2 hours of infection

the percentage of intracellular bacteria was significantly reduced upon *ppnK* knockdown, and the survival defect increased over time (Figure 5A), indicating that bacteria were not able to survive inside macrophages without proper NADK activity. We next investigated the role of ROS production by macrophages in the control of the Xen36/NADK sgRNA strain using the antioxidant agent N-acetyl cysteine (NAC). NAC partially restored bacterial survival (Figure 5A), indicating that the bacterial growth defect of the *ppnK* knockdown strain was in part due to its inability to cope with oxidative stress. Using fluorescence microscopy, we then investigated bacterial localization in macrophages 6 hours post-infection. Few Xen36/NADK sgRNA bacteria were detected compared to Xen36/pSD1 (Figure 5B), and NAC treatment led to an increased number of bacteria (Figure 5C), confirming bacterial enumeration results. Interestingly, while all knockdown bacteria colocalized with LAMP1, many Xen36/pSD1 bacteria did not upon NAC treatment, suggesting that NADK activity might be required for phagolysosome escape and bacterial survival in macrophages.

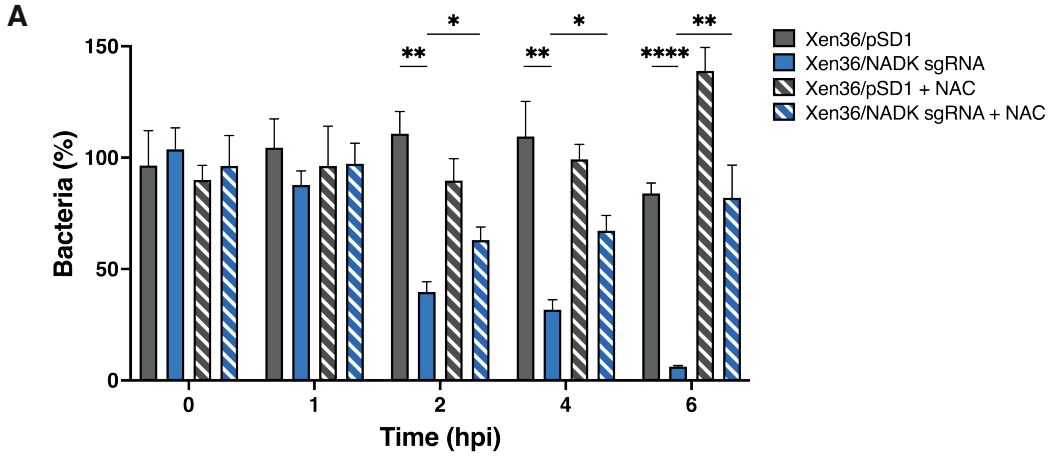

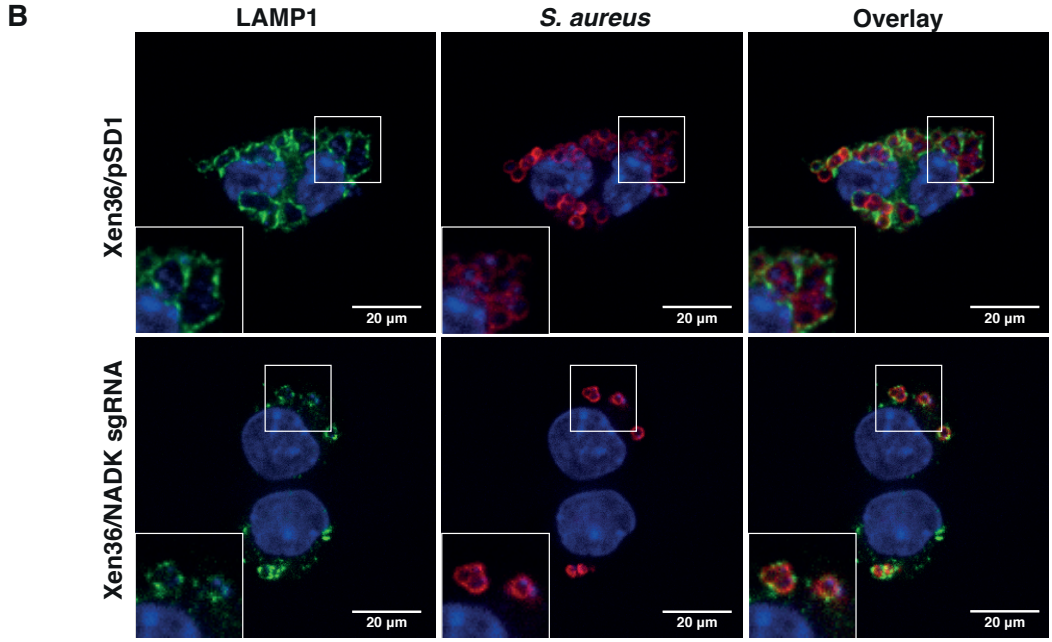

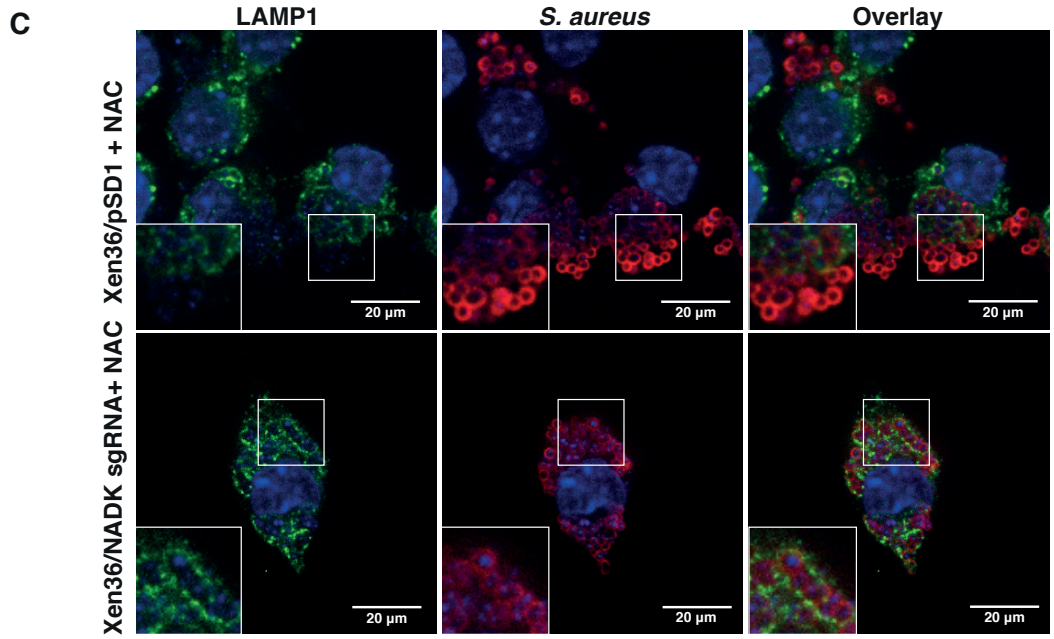

241

Figure 5 NADK promotes *S. aureus* survival in macrophages. (A) Percentage of growth of the *S. aureus* strain containing the empty vector (Xen36/pSD1) and the *ppnK* knock-down strain (Xen36/NADK sgRNA) at 0, 1, 2, 4 and 6 hours post-infection (hpi) of RAW264.7 macrophages left untreated or treated with N-acetylcysteine (NAC). Bars indicate standard errors of the means of biological replicates (n=4). Comparison of data was performed using two-ways analysis of variance (*p<0.05, **p<0.01, ****p<0.0001). (B-C) RAW264.7 macrophages were infected with Xen36/pSD1 or Xen36/NADK sgRNA and analyzed 6 hours post-infection by fluorescence microscopy using antibodies to label LAMP1 (FITC, green) and *S. aureus* (Cy5, red). Nuclei were labeled with DAPI (blue). B shows untreated macrophages. C shows macrophages treated with NAC. Images are representative of three independent experiments.

NADK promotes *S. aureus* virulence in zebrafish

Since phagocytes play a critical role in host defense against bacterial infection, we investigated whether NADK inhibition might influence *S. aureus* pathogenesis in a zebrafish infection model. This model allows short kinetics of infection (Prajsnar et al., 2008) and has been previously used to study *S. aureus* infection dynamics (Prajsnar et al., 2012). In addition to being optically transparent, zebrafish larvae innate immune system is the only one operating during the first days of development, facilitating the study of interactions between bacteria and neutrophils or macrophages. We first determined the stability of the pSD1 plasmid during infection. Zebrafish larvae were infected at 60 hours post fertilization (hpf) by intravenous injections of either the Xen36/pSD1 or Xen36/NADK sgRNA strains. Bacteria recovered from infected larvae were plated onto BHI agar with and without chloramphenicol. There was no significant difference between the number of bacteria growing on BHI alone and BHI supplemented with chloramphenicol up to 48 hours post-infection, irrespective of the strain (Figure supplement 3). Thus, plasmids were maintained in our experimental infection conditions. We next monitored zebrafish survival upon infection with 10^4 bacteria. Xen36/pSD1 infection led to ≈ 75% fish mortality at 24 hours post infection (Figure 6A). Strikingly, only one larva out of 48 died when bacterial NADK was inhibited (Figure 6A). Decreased fish mortality upon Xen36/NADK sgRNA infection was also observed 48 and 72

hours post-infection (Figure 6A). These results indicate that NADK inhibition leads to a decreased bacterial virulence. We then determined the bacterial burden of fish larvae 24 and 48 hours post-infection. Interestingly, we recovered similar amount of Xen36/pSD1 and Xen36/NADK sgRNA strains at both time points (Figure 6B), suggesting that NADK contributes to *S. aureus* pathogenic potential, which depends on both bacterial and host factors. As observed previously by Prasjnar et al. (Prajsnar et al., 2012), some fishes were able to control the infection with 10^4 bacteria but a high bacterial burden was associated with larval death in most cases (Figure 6B). In order to investigate the impact of NADK inhibition on phagocyte populations, we infected intravenously transgenic zebrafish lines with Xen36/pSD1 or Xen36/NADK sgRNA strains, and observed macrophages (Tg(*mfap4::mCherryF*)) and neutrophils (Tg(*mpx::GFP*)) 24 hours post-infection. Macrophages recruitment at the site of infection was observed for both strains (Figure 6C). We also noticed a strong depletion of neutrophils in larvae infected with Xen36/pSD1, while this neutropenia was more limited upon infection with NADK knockdown bacteria (Figure 6C). This correlated with the virulence differences of the two strains, given the key role of neutrophils in *S. aureus* infection (Pollitt et al., 2018; Prajsnar et al., 2012). Altogether, our results suggest that NADK is important for *S. aureus* pathogenesis.

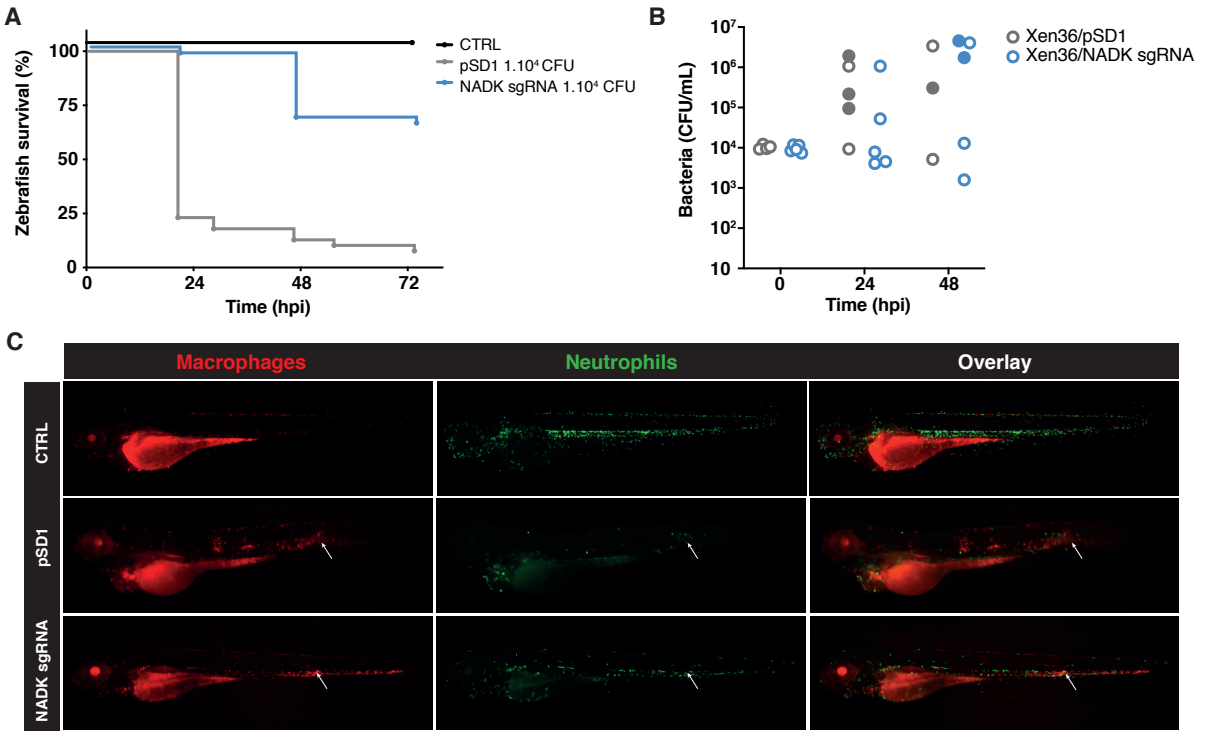

Figure 6 NADK contributes to *S. aureus* pathogenic potential in zebrafish. (A) Survival of zebrafish larvae intravenously injected at 60 hpf with 10^4 Xen36/pSD1 or Xen36/NADK sgRNA *S. aureus* (n=48). (B) Growth of Xen36/pSD1 or Xen36/NADK sgRNA *S. aureus* in zebrafish larvae upon intravenous injection with 10^4 bacteria. For each strain, CFU were determined in living larvae (open circles) or dead larvae (filled circles) 24 and 48 hours post-infection. (C) Homozygous Tg (*mfap4::mCherryF*) (ump6Tg) Tg(*mpx:GFP*) double transgenic fishes were infected intravenously with 10^4 Xen36/pSD1 or Xen36/NADK sgRNA *S. aureus* (arrows indicate the injection site). Macrophages (mCherry, red) and neutrophils (GFP, green) were imaged 24 hours post-infection.

Discussion

The ability of *S. aureus* to survive and thrive in a wide variety of niches during infection, ranging from skin to deeper tissues and abiotic devices, mirrors highly plastic metabolic capacities allowing adaptive responses to constantly changing microenvironments (Potter et al., 2020). Metabolic pathways are not only necessary for nutrient acquisition to sustain bacterial growth, but also for regulation of virulence and are therefore central to host-pathogen interactions (Eisenreich et al., 2010; Harper et al., 2018; Richardson, 2019; Teoh et al., 2021; Tomlinson et al., 2021).

Here we show for the first time that NADK contributes to bacterial pathogenic potential. NADK was necessary for successful *S. aureus* infection, ultimately leading to neutropenia and death of zebrafish larvae. Decreasing NADK activity led to decreased host mortality without affecting bacterial burden, suggesting that NADK promotes virulence factor activity and/or counteracts host defenses independently of its contribution to bacterial growth capacity. If the striking impact of NADK on mortality highlights its importance in the outcome of infection, future work will be necessary to decipher the role of the enzyme at each step of the infectious process. Besides neutrophils, macrophages are crucial cells in the innate immune defense against infection. We uncovered that inhibition of *S. aureus* NADK activity has a major impact on bacteria interactions with macrophages, reducing dramatically bacterial survival after phagocytosis. An important defense mechanism of macrophages against bacterial infection being the oxidative burst (Pidwill et al., 2021), we demonstrated that the role of NADK in *S. aureus* resistance to macrophage defenses was dependent on ROS levels. Along the same lines, we showed that NADK contributed to *S. aureus* resistance to hydrogen peroxide toxicity. NADK, as the only source of NADP(H), is a key component of defense against oxidative stress (Grose et al., 2006; Mailloux et al., 2011). In bacteria, it has been shown that NADK activity is increased upon exposure to oxidative stress, acting as a metabolic switch to decrease the NAD^+ pool which fuels ROS formation and increase the NADPH pool which promotes ROS scavenging activities (Singh et al., 2007). However, antioxidant treatment of infected macrophages using NAC only partially mitigated growth defect of the NADK knockdown strain. NADK might thus contribute to bacterial survival within macrophages through pathways other than ROS detoxification. We showed that inhibition of *ppnK* expression led to growth defect upon envelope stress, a condition that is encountered in the host and in particular in macrophages where bacteria face antimicrobial peptides (Rosenberger et al., 2004). If toxicity mediated by triclosan could be inhibited by

catalase treatment of the NADK knockdown strain, osmotic stress imposed by sodium chloride could not, confirming ROS-independent roles of NADK. NADP(H) is required in two reduction steps of fatty acid synthesis and its increased availability has been shown to increase fatty acid production in *Escherichia coli* (Li et al., 2018). NADK could thus contribute to *S. aureus* fitness by promoting functional fatty acid biosynthesis and maintenance of bacterial membrane integrity. Additionally, as NADP(H) is important for central metabolism, a defect in NADK activity might impair metabolic adaptation during infection. Virulence factors synthesis has been linked with TCA cycle and amino acids biosynthesis (Zhu et al., 2009). Thus decreased NADP(H) pools might modulate virulence factor synthesis and the fate of interactions with host cells.

Although its activity is highly conserved in almost all living organisms, prokaryotes and human NADK are significantly different (Lerner et al., 2001). Furthermore, NADK catalytic site adopt a specific conformation in comparison to other NAD-binding enzymes (Petrelli et al., 2009). NADK, whose activity is essential for growth, is thus an interesting target for antibiotic development. Using a fragment-based drug design approach, we previously developed a family of chemical compounds targeting bacterial NADK (Gelin et al., 2012; Paoletti et al., 2016). A lead compound, NKI1, limited the growth of both methicillin sensitive and methicillin resistant *S. aureus* strains *in vitro* but also in a mouse model of infection, without any signs of toxicity (Gelin et al., 2020). The anti-infective activity of NKI1 could thus rely on its capacity to inhibit NADK-mediated bacterial stress response and virulence in addition to metabolic pathways. Interestingly, we found that inhibition of NADK could potentiate the toxicity of polymyxin B, levofloxacin, kanamycin and rifampicin in a ROS-dependent manner. Although controversial, ROS-production has been proposed as a common antibiotic-mediated killing mechanism (Baquero and Levin, 2020; Van Acker and Coenye, 2017). Polymyxins have been suggested to permeabilize and/or

disrupt membranes of Gram-negative bacteria. They also induce ROS production through TCA cycle activation (Yin et al., 2020). ROS have been shown to contribute to bactericidal activity of quinolone antibiotics (Kottur and Nair, 2016). Both quinolones and aminoglycosides promote ROS formation mediated by TCA and NADH depletion (Belenky et al., 2015; Kohanski et al., 2007, 2010). Thus, ROS may account for antibiotic potentiation by NADK inhibitors. In addition, non-oxidative mechanisms contribute to potentiation, as NADK contributed to resistance to vancomycin in a ROS-independent manner. It would be interesting to investigate potential synergy between classical antibiotic families and NADK inhibition, especially in the context of antibiotic resistance.

Further investigations are now required to fully decipher the contribution of bacterial NADKs during infection processes and develop optimized NADK inhibitors that could be used in combination with current antibiotics to fight multidrug resistant bacteria.

Materials and methods

Synteny analysis

Comparative analysis of the *ppnK* genomic locus was conducted in *Bacilli* using *S. aureus ppnK* gene (SAOUHSC_00943) as input on the web server SyntTax (Oberto, 2013). Generated PDF files were edited to rename genes and remove genes outside of synteny for clarity.

Plasmids, bacterial strains, cell lines and culture conditions

Bacterial strains and plasmids used in this study are listed in Table 1. All plasmids were maintained in *Escherichia coli* TOP10. The restriction deficient *Staphylococcus aureus* strain RN4220 was transformed with plasmids isolated from *E. coli*. The *S. aureus* Xen36 strain was transformed with plasmids isolated from the RN4220 strain as previously described (Gelin et

al., 2020). *E. coli* was grown in lysogeny broth (LB) medium (Difco) with shaking at 200 rpm or on LB agar plates at 37°C. *S. aureus* was grown in brain heart infusion (BHI) broth (BD) or in tryptic soy broth (TSB) (Difco) with shaking at 200 rpm or on BHI agar plates at 37°C. When required, culture medium was supplemented with antibiotics (carbenicillin 100 µg/mL for *E. coli*, chloramphenicol 15 µg/mL or anhydrotetracycline 100 ng/mL for *S. aureus*). RAW 264.7 macrophages (TIB-71, ATCC) were cultured in DMEM (Gibco) containing 10 % FCS (Gibco). Macrophages were seeded into 24-well plates at 10^5 cells per well.

Table 1 Strains and plasmids used in this study.

Strain/plasmid	Relevant characteristics	Reference
Strains		
***E. coli* strain**		
TOP10	F⁻*mcrA* Δ*(mrr-hsdRMS-mcrBC)* ϕ80*lacZ*Δ*M15* Δ*lacX74 recA1 araD139* Δ*(ara-leu) 7697 galU galK* λ⁻ *rpsL*(Str^R) *endA1 nupG*	Invitrogen
***S. aureus* strains**		
Xen36	Strain derived from a clinical isolate from a bacteremic patient (ATCC 49525)	Caliper Life Science
Xen36/pSD1	Xen36 strain carrying plasmid pSD1	(Gelin et al., 2020)
Xen36/NADK sgRNA	Xen36 strain carrying plasmid pSD1 *ppnK*	(Gelin et al., 2020)
RN4220	Restriction-deficient strain derived from NCTC 8325-4	(Kreiswirth et al., 1983)
Plasmids		
pSD1	dCas9 ATc-inducible expression and sgRNA constitutive expression plasmid	(Zhao et al., 2017)
pSD1 *ppnK*	pSD1 plasmid carrying sgRNA targeting *S. aureus ppnK*	(Gelin et al., 2020)

Table 2 Primers used in this study

Primer	Sequence (5'-3')
RT-ppnK-F	GTGACTCCAAGTCTAATGCC
RT-ppnK-R	ATTTTTCAACTTCATGAGGTAACC
RT-operon-F1	TGACTTGCTTAAAAAGCACACTG
RT-operon-R1	ACGAGCATTTGTCCTACTTCAGA
RT-operon-F2	AACCGTTGAAGAAACATTCGACA
RT-operon-R2	GACGCTTGTTCACCAACTTCA
RT-operon-F3	CATCGTTTGGAAAGAGCGGC
RT-operon-R3	GGCATTAGACTTGGAGTCACCT
RT-operon-F4	ACGTGTGCACGATTCTTTCAT
RT-operon-R4	ATGGCGCTCACTGTCTTCT
RT-operon-F5	AGTTCATTTGCATACGGGACG
RT-operon-R5	ACGCTCTTTTTCATCTGTGTTCA
RT-operon-F6	TAACTTGTGCGATGACGGTGG
RT-operon-R6	TTCCAATCACAATCCCCATCAA
RT-operon-F7	ACGTTGATGAATTGAAGCAAGAG
RT-operon-R7	ACTTTAGCGACACCAAAAGCA
RT-operon-F8	TCAAGTGGCGTTACAGGTGA
RT-operon-R8	TTCAAATACCGCCAACGCAT

391

392 **Bacterial growth measurement**

393 *S. aureus* strains were grown overnight in BHI broth at 37°C and diluted to OD_{600nm}=0.05 into
394 BHI broth. For NADK inhibition experiments, culture medium was supplemented with 100
395 ng/mL anhydrotetracycline (Sigma-Aldrich) and 15 µg/mL chloramphenicol when required.
396 For stress experiments, culture medium was supplemented at indicated concentrations with
397 hydrogen peroxide, triton X-100, polymyxin B, kanamycin, rifampicin, vancomycin (Sigma-
398 Aldrich), triclosan, sodium chloride (Merck) or levofloxacin (USP). Bacterial suspensions
399 were incubated in 96-well plates with shaking at 200 rpm at 37°C. Growth was monitored
400 with a microplate reader (Glomax Discover, Promega). Experiments were performed at least
401 three times.

402

403 **RNA extraction and RT-PCR**

404 Bacteria grown for 4 h were collected by centrifugation 20 min at 15,000 x *g* at 4°C. Bacterial
405 lysis was performed using Precellys lysing kit (P000914-LYSK0-A) and the Precellys
406 program 4 (6.500 rpm for 30 sec) twice at 4°C. RNA extraction was performed in 1 mL of
407 TRIzol (Invitrogen) according to the manufacturer's recommendations. RT-PCR was carried
408 out with Superscript one step RT kit (Invitrogen). Primers used are indicated in Table 2. RT-
409 PCR assays were repeated at least 3 times.

410

411 **Immunoblotting**

412 Bacteria grown for 4 h were collected by centrifugation 10 min at 10,000 x *g* at 4° C and
413 resuspended in 500 µL of PBS. Bacteria were lysed using the Precellys lysing kit (P000914-
414 LYSK0-A) and the Precellys program 4 (6,500 rpm for 30 sec) twice at 4°C. Lysates were
415 centrifuged for 15 min at 10,000 x *g* at 4 °C and supernatants were collected for protein

quantification using the Quick start Bradford protein assay kit 2 (Biorad). Samples were mixed with Laemmli buffer (Biorad) and 10% β-mercaptoethanol and denatured for 5 min at 95°C. Samples were separated onto 4−20% Miniprotean TGX stain-free precast gel (Biorad) in TGS buffer and transferred on polyvinylidene fluoride membranes. Membranes were incubated overnight at 4°C with primary antibodies diluted in 5% blotto (R114 rabbit anti-EF-Tu polyclonal antibodies, 1:5000; R250 rabbit polyclonal anti-*S. aureus* NADK antibodies, 1:1000). Membranes were then incubated with 1:2500 antirabbit horseradish peroxidase-conjugated antibodies (Abcam). Blots were revealed using the ECL kit (Pierce).

Negative staining

S. aureus were fixed with 2.5% glutaraldehyde in culture medium for 1 h at room temperature and stored overnight at 4°C before processing. Fixed bacteria were adsorbed to 300-mesh Formvar-Cu-coated grids treated with 1% alcian blue (Sigma-Aldrich) (Lang et al., 1981) (Electron Microscopy Science) for 20 min. Grids were rinsed three times with ultrapure water and stained for 1 min with 2% aqueous uranyl acetate, washed again for three times with ultrapure water and dried. Images were recorded with a TECNAI SPIRIT 120 kV transmission electron microscope equipped with a bottom-mounted EAGLE 4Kx4K camera (FEI-Thermofisher Company).

Scanning electron microscopy

Chemically fixed *S. aureus* were washed in 0.1 M HEPES buffer pH 7.2, postfixed for 1 h in 1% osmium tetroxide in 0.1 M HEPES buffer pH 7.2, and rinsed with distilled water. Samples were dehydrated through a graded series of 25, 50, 75, 95 and 100% ethanol solution followed by critical point drying with CO_2 (CPD300 LEICA). Dried specimens were sputtered with 20 nm gold palladium, with a GATAN ion beam coater, and were observed with an AURIGA

field emission scanning electron microscope operating at 5 kV (Carl Zeiss, Inc.). Images were acquired with the secondary electron detector.

Transmission electron microscopy

Chemically fixed *S. aureus* were washed in HEPES buffer pH 7.2, postfixed with 1% osmium tetroxide in 0.1M HEPES buffer pH 7.2 for 1 h and washed three times with distilled water. Samples were resuspended in Agar-type-IX 4% solution (Sigma) and allowed to solidify on ice, dehydrated in a graded series of ethanol and embedded in epoxy resin. After polymerization, thin sections were cut with a Leica Ultramicrotome Ultracut UC7' sections (60 nm), stained with uranyl acetate and lead citrate. Images were recorded with TECNAI SPIRIT 120 kV transmission electron microscope equipped with a bottom-mounted EAGLE 4Kx4K camera (FEI-Thermofisher Compagny).

RAW 264.7 macrophage infection

RAW 264.7 macrophages were seeded into 24-well plates at 100,000 cells per well. *S. aureus* Xen36/pSD1 and *S. aureus* Xen36/NADK sgRNA strains were grown to an OD_{600nm} of 0.6, washed three times and diluted in DMEM to obtain a multiplicity of infection (MOI) of 10. Infected macrophages were centrifugated at 500 x *g* for 5 min and incubated for 15 min at 37°C and 5% CO_2 to synchronize phagocytosis. The medium was replaced with DMEM containing gentamicin (20 µg/mL) for 30 min to kill extracellular bacteria. Cells were washed three times in DPBS and incubated in DMEM supplemented with 100 ng/mL anhydrotetracycline and 10 mM N-acetyl cysteine (NAC, Sigma-Aldrich) when indicated. Cells were incubated for 6 h at 37°C and 5% CO_2. At each time points, cells were lysed in 0.2% Triton X-100 for 10 min at 37°C. The number of bacteria released from the cells was

465 determined by plating serial dilutions of the lysates on BHI agar plates that were incubated at
466 37°C for colony-forming units (CFU) enumeration.
467
468 **Immunofluorescence assay**
469 RAW 264.7 macrophages were cultured on glass coverslips in 24-well plates. At 6 h post-
470 infection, cells were fixed in paraformaldehyde (PFA) 4% for 15 min, permeabilized for 4
471 min with 0.1% Triton X-100 in 1% bovine serum albumin (BSA)-PBS and blocked in 1%
472 BSA-PBS. Fixed cells were incubated for 30 min with rabbit anti-*S. aureus* (Abcam ab20920)
473 and rat anti-LAMP1 1D4B (Abcam ab25245) primary antibodies. Cells were then incubated
474 for 30 min with goat anti-rabbit Cy5 (Immunoresearch 111 175 144) or goat anti-rat FITC
475 (Invitrogen A11006) secondary antibodies and DAPI (10 µg/mL). Slides were mounted with
476 Fluoromount G (Invitrogen). Samples were observed with a Zeiss Axiovert 200M
477 epifluorescence microscope equipped with a Plan-apochromat objective (100X/1.4 Oil Ph3;
478 Carl Zeiss, Inc.). Images were acquired with a CCD camera Coolsnap, processed with
479 Metamorph software v.6 (Molecular Devices) and analyzed with ImageJ software.
480
481 **Ethics Statement**
482 Animal experiments were performed according to European Union guidelines for handling of
483 laboratory animals (http://ec.europa.eu/environment/chemicals/lab_animals/home_en.htm).
484 All experiments performed on larvae older than 5 days post fertilization were approved by the
485 Institut Pasteur Animal Care and Use Committee and the French Ministry of Education,
486 Research and Innovation, and registered under the reference APAFIS#31827.
487
488 **Zebrafish care and maintenance**
489 Homozygous Tg*(mfap4::mCherryF)* (ump6Tg) (Phan et al., 2018) Tg(*mpx::GFP*)^{i114}
490 (Renshaw et al., 2006) double transgenic fishes were raised in our facility. Eggs were

obtained by natural spawning, bleached according to standard protocols, and then kept in Petri dishes containing Volvic spring water and, from 24 h post fertilization (hpf) onwards, 0.003% 1-phenyl-2-thiourea (PTU) (Sigma-Aldrich) was added to prevent pigmentation. Embryos were reared at 28°C or 24°C according to the desired speed of development; infected larvae were always kept at 28°C. All timings in the text refer to the developmental stage at the reference temperature of 28°C. Larvae were anesthetized with 200 μg/ml tricaine (Sigma-Aldrich) during the injection procedure as well as during *in vivo* imaging and processing for bacterial burden evaluation.

Zebrafish infection

The volume of injected bacterial suspension was deduced from the diameter of the drop obtained after mock microinjection, as described in (Levraud et al., 2008). Bacteria were diluted from overnight cultures and allowed to reach exponential growth. Then, they were recovered by centrifugation, washed and resuspended at the desired concentration in PBS. 55-60 hours post-fertilization, anesthetized zebrafish larvae were microinjected intravenously (IV) with 1 nL of bacterial suspension at the desired dose as described (Colucci-Guyon et al., 2011; Mostowy et al., 2013). Infected larvae were transferred into individual wells containing 1 mL of Volvic water and 0.003% PTU in 24-well culture plates, incubated at 28°C and regularly observed under a stereomicroscope.

Evaluation of the bacterial burden in infected zebrafish larvae

Infected zebrafish larvae were collected at 0, 24, 48 and 72 hours post infection (hpi) and lysed for the evaluation of the bacterial burden as previously described (Boucontet et al., 2018; Mostowy et al., 2013). Each larva was placed in an individual 1.5 mL Eppendorf tube and anesthetized with tricaine (200 μg/mL), washed with 1 mL of sterile water and placed in

150 µL of sterile water. Larvae were then homogenized using a pestle motor mixer (Argos). Each sample was transferred to an individual well of a 96-well plate and 10 X serial dilutions were performed. For CFU enumeration and to assess plasmid stability throughout the infection kinetics, serial dilutions of lysates were plated on BHI agar plates with and without chloramphenicol (15 µg/mL) that were incubated at 37°C.

Zebrafish live imaging, image processing and analysis

Quantification of total macrophages and neutrophils on living transgenic reporter larvae was performed upon infection as we previously described (Mostowy et al., 2013). Briefly, bright field, GFP and RFP images of whole living anesthetized larvae were taken using a Leica Macrofluo™ Z16 APOA (zoom 16:1) macroscope equipped with a Leica PlanApo 2.0X lens, and a Photometrics® CoolSNAP™ *HQ2* camera. Images were captured using the Metavue software version 7.5.6.0 (MDS Analytical Technologies). After capture of images, larvae were washed and transferred in a new 24-well plate filled with 1 mL of fresh water in each well and incubated at 28°C.

Statistical analysis

Results are expressed as means ± SEM of at least 3 replicates. Statistical analysis was performed using GraphPad Prism (GraphPad Prism® 9.1.2. Software). One-way or two-ways ANOVA were used to compare data. Differences between groups were considered significant when the *p* value was lower than 0.05. Survival data were plotted using the Kaplan-Meier estimator and log-rank (Mantel-Cox) tests were performed to assess differences between groups.

Aknowlegments

We thank Changlong Zhao for providing pSD1. We are grateful to all members of the *Yersinia* research unit and the French national reference center for plague and other yersiniosis, the members of the NADkiller consortium as well as Frédéric Barras and Daniel Ladant for helpful discussions and insightful comments. We also wish to thank the members of the fish facility team Yohann Rolin and Noël Aimar for their excellent care of the fish.

This work was funded by the Agence Nationale de la Recherche (grant ANR-17-CE18-0011-02) and supported by Institut Pasteur, Université de Paris and CNRS. The *Yersinia* Research Unit and the Macrophages and Immunity Development Unit are members of the Laboratory of Excellence Integrative Biology of Emerging Infectious Diseases (ANR-10-LBX-62-IBEID). We are grateful for support for equipment from the French government Programme d'investissements d'avenir France BioImaging (ANR-10-INSB-04-01).

Competing interests

The authors declare no conflict of interest.

References

Avican K, Aldahdooh J, Togninalli M, Mahmud AKMF, Tang J, Borgwardt KM, Rhen M, Fällman M. 2021. RNA atlas of human bacterial pathogens uncovers stress dynamics linked to infection. *Nat Commun* **12**. doi:10.1038/S41467-021-23588-W

Baquero F, Levin BR. 2020. Proximate and ultimate causes of the bactericidal action of antibiotics. *Nat Rev Microbiol*. **19**:123-132. doi:10.1038/s41579-020-00443-1

Belenky P, Ye JD, Porter CBM, Cohen NR, Lobritz MA, Ferrante T, Jain S, Korry BJ, Schwarz EG, Walker GC, Collins JJ. 2015. Bactericidal antibiotics induce toxic metabolic perturbations that lead to cellular damage. *Cell Rep* **13**:968–980. doi:10.1016/j.celrep.2015.09.059

Berrin JG, Pierrugues O, Brutesco C, Alonso B, Montillet JL, Roby D, Kazmaier M. 2005. Stress induces the expression of AtNADK-1, a gene encoding a NAD(H) kinase in *Arabidopsis thaliana*. *Mol Genet Genomics* **273**:10–19. doi:10.1007/s00438-005-1113-1

Boucontet L, Passoni G, Thiry V, Maggi L, Herbomel P, Levraud J-P, Colucci-Guyon E. 2018. A model of superinfection of virus-infected zebrafish larvae: increased susceptibility to bacteria associated with neutrophil death. *Front Immunol* **9**:1084. doi:10.3389/FIMMU.2018.01084

Chai M-F, Wei P-C, Chen Q-J, An R, Chen J, Yang S, Wang X-C. 2006. NADK3, a novel cytoplasmic source of NADPH, is required under conditions of oxidative stress and modulates abscisic acid responses in *Arabidopsis*. *Plant J* **47**:665–674. doi:10.1111/j.1365-313X.2006.02816.x

Chandel NS. 2021. Carbohydrate Metabolism. *Cold Spring Harb Perspect Biol* **13**:1–15. doi:10.1101/CSHPERSPECT.A040568

Chaudhuri RR, Allen AG, Owen PJ, Shalom G, Stone K, Harrison M, Burgis TA, Lockyer M,

582 Garcia-Lara J, Foster SJ, Pleasance SJ, Peters SE, Maskell DJ, Charles IG. 2009.
583 Comprehensive identification of essential *Staphylococcus aureus* genes using
584 Transposon-Mediated Differential Hybridisation (TMDH). *BMC Genomics* **10**:291.
585 doi:10.1186/1471-2164-10-291
586 Chini CCS, Zeidler JD, Kashyap S, Warner G, Chini EN. 2021. Evolving concepts in NAD+
587 metabolism. *Cell Metab*. **33**:1076-1087. doi:10.1016/j.cmet.2021.04.003
588 Colucci-Guyon E, Tinevez J-Y, Renshaw SA, Herbomel P. 2011. Strategies of professional
589 phagocytes in vivo: unlike macrophages, neutrophils engulf only surface-associated
590 microbes. *J Cell Sci* **124**:3053–3059. doi:10.1242/JCS.082792
591 Covarrubias AJ, Perrone R, Grozio A, Verdin E. 2021. NAD^+ metabolism and its roles in
592 cellular processes during ageing. *Nat Rev Mol Cell Biol*. **22**:119–141.
593 doi:10.1038/s41580-020-00313-x
594 Eisenreich W, Dandekar T, Heesemann J, Goebel W. 2010. Carbon metabolism of
595 intracellular bacterial pathogens and possible links to virulence. *Nat Rev Microbiol*
596 **8**:401–412. doi:10.1038/NRMICRO2351
597 Fang FC, Frawley ER, Tapscott T, Vázquez-Torres A. 2016. Bacterial stress responses during
598 host infection. *Cell Host Microbe* **20**:133–143. doi:10.1016/J.CHOM.2016.07.009
599 Fisher DJ, Fernandez RE, Maurelli AT. 2013. *Chlamydia trachomatis* transports NAD via the
600 Npt1 ATP/ADP translocase. *J Bacteriol* **195**:3381-3386. doi:10.1128/JB.00433-13
601 Galione A, Chuang K-T. 2020. Pyridine nucleotide metabolites and calcium release from
602 intracellular stores. *Adv Exp Med Biol* **1131**:371–394. doi:10.1007/978-3-030-12457-
603 1_15
604 Gelin M, Paoletti J, Huteau V, Nahori M, Leseigneur C, Dugue L, Clement D, Pons J, Assairi
605 L, Pochet S, Labesse G, Dussurget O. 2020. From substrate to fragments to inhibitor
606 active in vivo against *Staphylococcus aureus*. *ACS Infect Dis* **6**:422–435.

607 doi:10.1021/acsinfecdis.9b00368

608 Gelin M, Poncet-Montange G, Assairi L, Morellato L, Huteau V, Dugué L, Dussurget O,
609 Pochet S, Labesse G. 2012. Screening and in situ synthesis using crystals of a NAD
610 kinase lead to a potent antistaphylococcal compound. *Structure*. **20**:1107-17.
611 doi:10.1016/j.str.2012.03.024

612 Grose H., Joss L, Velick SF, Roth JR. 2006. Evidence that feedback inhibition of NAD kinase
613 controls responses to oxidative stress. *Proc Natl Acad Sci USA* **103**:7601–7606.
614 doi:10.1073/pnas.0602494103

615 Guillén J, Bernabeu A, Shapiro S, Villalaín J. 2004. Location and orientation of Triclosan in
616 phospholipid model membranes. *Eur Biophys J* **33**:448–453. doi:10.1007/S00249-003-
617 0378-8

618 Harper L, Balasubramanian D, Ohneck EA, Sause WE, Chapman J, Mejia-Sosa B, Lhakhang
619 T, Heguy A, Tsirigos A, Ueberheide B, Boyd JM, Lun DS, Torres VJ. 2018.
620 *Staphylococcus aureus* responds to the central metabolite pyruvate to regulate virulence.
621 *mBio* **9**:2272–2289. doi:10.1128/mBio.02272-17

622 Jarrett HW, Charbonneau H, Anderson JM, McCann RO, Cormier MJ. 1980. Plant
623 calmodulin and the regulation of NAD kinase. *Ann N Y Acad Sci*. **356**: 119-29.

624 Kawai S, Mori S, Mukai T, Suzuki S, Yamada T, Hashimoto W, Murata K. 2000. Inorganic
625 polyphosphate/ATP-NAD kinase of *Micrococcus flavus* and *Mycobacterium*
626 *tuberculosis* H37Rv. *Biochem Biophys Res Commun* **276**:57–63.
627 doi:10.1006/bbrc.2000.3433

628 Kobayashi K, Ehrlich SD, Albertini A, Amati G, Andersen KK, Arnaud M, Asai K, Ashikaga
629 S, Aymerich S, Bessieres P, Boland F, Brignell SC, Bron S, Bunai K, Chapuis J,
630 Christiansen LC, Danchin A, Débarbouillé M, Dervyn E, Deuerling E, Devine K, Devine
631 SK, Dreesen O, Errington J, Fillinger S, Foster SJ, Fujita Y, Galizzi A, Gardan R,

632 Eschevins C, Fukushima T, Haga K, Harwood CR, Hecker M, Hosoya D, Hullo MF,
633 Kakeshita H, Karamata D, Kasahara Y, Kawamura F, Koga K, Koski P, Kuwana R,
634 Imamura D, Ishimaru M, Ishikawa S, Ishio I, le Coq D, Masson A, Mauël C, Meima R,
635 Mellado RP, Moir A, Moriya S, Nagakawa E, Nanamiya H, Nakai S, Nygaard P, Ogura
636 M, Ohanan T, O'Reilly M, O'Rourke M, Pragai Z, Pooley HM, Rapoport G, Rawlins JP,
637 Rivas LA, Rivolta C, Sadaie A, Sadaie Y, Sarvas M, Sato T, Saxild HH, Scanlan E,
638 Schumann W, Seegers JFML, Sekiguchi J, Sekowska A, Séror SJ, Simon M, Stragier P,
639 Studer R, Takamatsu H, Tanaka T, Takeuchi M, Thomaides HB, Vagner V, van Dijl JM,
640 Watabe K, Wipat A, Yamamoto H, Yamamoto M, Yamamoto Y, Yamane K, Yata K,
641 Yoshida K, Yoshikawa H, Zuber U, Ogasawara N. 2003. Essential *Bacillus subtilis*
642 genes. *Proc Natl Acad Sci USA* **100**:4678–4683. doi:10.1073/pnas.0730515100

643 Kohanski MA, Dwyer DJ, Collins JJ. 2010. How antibiotics kill bacteria: from targets to
644 networks. *Nat Rev Microbiol* **8**:423–435. doi:10.1038/nrmicro2333

645 Kohanski MA, Dwyer DJ, Hayete B, Lawrence CA, Collins JJ. 2007. A common mechanism
646 of cellular death induced by bactericidal antibiotics. *Cell* **130**:797–810.
647 doi:10.1016/j.cell.2007.06.049

648 Kornberg A. 1950. Enzymatic synthesis of triphosphopyrine nucleotide. *J Biol Chem*
649 **182**:805–813.

650 Kottur J, Nair DT. 2016. Reactive Oxygen Species play an important role in the bactericidal
651 activity of quinolone antibiotics. *Angew Chem Int Ed Engl* **55**:2397–2400.
652 doi:10.1002/ANIE.201509340

653 Kreiswirth BN, Löfdahl S, Betley MJ, O'Reilly M, Schlievert PM, Bergdoll MS, Novick RP.
654 1983. The toxic shock syndrome exotoxin structural gene is not detectably transmitted
655 by a prophage. *Nature* **305**:709–712. doi:10.1038/305709a0

656 Lang RD, Nermut M V, Williams LD. 1981. Ultrastructure of sheep erythrocyte plasma

membranes and cytoskeletons bound to solid supports. *J Cell Sci* **49**:383–99.

Lerner F, Niere M, Ludwig A, Ziegler M. 2001. Structural and functional characterization of human NAD kinase. *Biochem Biophys Res Commun* **288**:69–74. doi:10.1006/bbrc.2001.5735

Levraud J-P, Colucci-Guyon E, Redd MJ, Lutfalla G, Herbomel P. 2008. *In vivo* analysis of zebrafish innate immunity. *Methods Mol Biol* **415**:337–363. doi:10.1007/978-1-59745-570-1_20

Li B Bin, Wang X, Tai L, Ma TT, Shalmani A, Liu WT, Li WQ, Chen KM. 2018. NAD kinases: Metabolic targets controlling redox co-enzymes and reducing power partitioning in plant stress and development. *Front Plant Sci*. **9**:379. doi:10.3389/fpls.2018.00379

Li W, Wu H, Li M, San KY. 2018. Effect of NADPH availability on free fatty acid production in *Escherichia coli*. *Biotechnol Bioeng* **115**:444–452. doi:10.1002/bit.26464

Love NR, Pollak N, Dölle C, Niere M, Chen Y, Oliveri P, Amaya E, Patel S, Ziegler M. 2015. NAD kinase controls animal NADP biosynthesis and is modulated via evolutionarily divergent calmodulin-dependent mechanisms. *Proc Natl Acad Sci USA* **112**:1386–91. doi:10.1073/pnas.1417290112

Lu H, Tonge PJ. 2008. Inhibitors of FabI, an enzyme drug target in the bacterial fatty acid biosynthesis pathway. *Acc Chem Res* **41**:11–20. doi:10.1021/ar700156e

Mailloux RJ, Lemire J, Appanna VD. 2011. Metabolic networks to combat oxidative stress in *Pseudomonas fluorescens*. *Antonie van Leeuwenhoek* **99**:433–442. doi:10.1007/s10482-010-9538-x

McGuinness ET, Butler JR. 1985. NAD+ kinase - a review. *Int J Biochem* **17**:1–11.

Mostowy S, Boucontet L, Mazon Moya MJ, Sirianni A, Boudinot P, Hollinshead M, Cossart P, Herbomel P, Levraud JP, Colucci-Guyon E. 2013. The zebrafish as a new model for the *in vivo* study of *Shigella flexneri* interaction with phagocytes and bacterial

682 autophagy. *PLoS Pathog* **9**:12–16. doi:10.1371/journal.ppat.1003588

683 Muto S, Miyachi S. 1977. Properties of a protein activator of NAD kinase from plants. *Plant*
684 *Physiol* **59**:55–60. doi:10.1104/pp.59.1.55

685 Oberto J. 2013. SyntTax: A web server linking synteny to prokaryotic taxonomy. *BMC*
686 *Bioinformatics* **14**. doi:10.1186/1471-2105-14-4

687 Paoletti J, Assairi L, Gelin M, Huteau V, Nahori MA, Dussurget O, Labesse G, Pochet S.
688 2016. 8-Thioalkyl-adenosine derivatives inhibit *Listeria monocytogenes* NAD kinase
689 through a novel binding mode. *Eur J Med Chem* **124**:1041–1056.
690 doi:10.1016/j.ejmech.2016.10.033

691 Petrelli R, Sham YY, Chen L, Felczak K, Bennett E, Wilson D, Aldrich C, Yu JS, Cappellacci
692 L, Franchetti P, Grifantini M, Mazzola F, Di Stefano M, Magni G, Pankiewicz KW.
693 2009. Selective inhibition of nicotinamide adenine dinucleotide kinases by dinucleoside
694 disulfide mimics of nicotinamide adenine dinucleotide analogues. *Bioorganic Med Chem*
695 **17**:5656–5664. doi:10.1016/j.bmc.2009.06.013

696 Phan QT, Sipka T, Gonzalez C, Levraud J-P, Lutfalla G, Nguyen-Chi M. 2018. Neutrophils
697 use superoxide to control bacterial infection at a distance. *PLoS Pathog* **14**:e1007157.
698 doi:10.1371/JOURNAL.PPAT.1007157

699 Pidwill GR, Gibson JF, Cole J, Renshaw SA, Foster SJ. 2021. The role of macrophages in
700 *Staphylococcus aureus* infection. *Front Immunol* **11**:3506.
701 doi:10.3389/fimmu.2020.620339

702 Pollitt EJG, Szkuta PT, Burns N, Foster SJ. 2018. *Staphylococcus aureus* infection dynamics.
703 *PLoS Pathog* **14**:e1007112. doi:10.1371/journal.ppat.1007112

704 Potter AD, Butrico CE, Ford CA, Curry JM, Trenary IA, Tummarakota SS, Hendrix AS,
705 Young JD, Cassat JE. 2020. Host nutrient milieu drives an essential role for aspartate
706 biosynthesis during invasive *Staphylococcus aureus* infection. *Proc Natl Acad Sci USA*

117:12394–12401. doi:10.1073/pnas.1922211117

Prajsnar TK, Cunliffe VT, Foster SJ, Renshaw SA. 2008. A novel vertebrate model of *Staphylococcus aureus* infection reveals phagocyte-dependent resistance of zebrafish to non-host specialized pathogens. *Cell Microbiol* **10**:2312–2325. doi:10.1111/j.1462-5822.2008.01213.x

Prajsnar TK, Hamilton R, Garcia‐Lara J, McVicker G, Williams A, Boots M, Foster SJ, Renshaw SA. 2012. A privileged intraphagocyte niche is responsible for disseminated infection of *Staphylococcus aureus* in a zebrafish model. *Cell Microbiol* **14**:1600–1619. doi:10.1111/j.1462-5822.2012.01826.x

Renshaw SA, Loynes CA, Trushell DMI, Elworthy S, Ingham PW, Whyte MKB. 2006. A transgenic zebrafish model of neutrophilic inflammation. *Blood* **108**:3976–3978. doi:10.1182/BLOOD-2006-05-024075

Richardson AR. 2019. Virulence and metabolism. *Microbiol Spectr* **7**. doi:10.1128/microbiolspec.gpp3-0011-2018

Rosenberger CM, Gallo RL, Finlay BB. 2004. Interplay between antibacterial effectors: a macrophage antimicrobial peptide impairs intracellular *Salmonella* replication. *Proc Natl Acad Sci USA* **101**:2422-7. doi:10.1073/pnas.0304455101

Ruiz JM, Sánchez E, García PC, López-Lefebre LR, Rivero RM, Romero L. 2002. Proline metabolism and NAD kinase activity in greenbean plants subjected to cold-shock. *Phytochemistry* **59**:473–478. doi:10.1016/S0031-9422(01)00481-2

Sassetti CM, Boyd DH, Rubin EJ. 2003. Genes required for mycobacterial growth defined by high density mutagenesis. *Mol Microbiol* **48**:77–84. doi:10.1046/j.1365-2958.2003.03425.x

Simon P, Dieter P, Bonzon M, Greppin H, Marmé D. 1982. Calmodulin-dependent and independent NAD kinase activities from cytoplasmic and chloroplastic fractions of

spinach (*Spinacia oleracea* L.). *Plant Cell Rep* **1**:119-122. doi:10.1007/BF00272368

Singh R, Mailloux RJ, Puiseux-Dao S, Appanna VD. 2007. Oxidative stress evokes a metabolic adaptation that favors increased NADPH synthesis and decreased NADH production in *Pseudomonas fluorescens*. *J Bacteriol* **189**:6665–6675. doi:10.1128/JB.00555-07

Ślaski JJ. 1995. NAD+ kinase activity in root tips of nearly isogenic linesof wheat (*Triticum aestivum* L.) that differ in their tolerance to aluminium. *J Plant Physiol* **145**:143–147. doi:10.1016/S0176-1617(11)81861-4

Tai L, Li B-B, Nie X-M, Zhang P-P, Hu C-H, Zhang L, Liu W-T, Li W-Q, Chen K-M. 2019. Calmodulin is the fundamental regulator of NADK-mediated NAD signaling in plants. *Front Plant Sci* **10**:681. doi:10.3389/fpls.2019.00681

Teoh WP, Chen X, Laczkovich I, Alonzo F 3rd. 2021. *Staphylococcus aureus* adapts to the host nutritional landscape to overcome tissue-specific branched-chain fatty acid requirement. *Proc Natl Acad Sci USA* **118**. doi:10.1073/PNAS.2022720118

Tomlinson KL, Lung TWF, Dach F, Annavajhala MK, Gabryszewski SJ, Groves RA, Drikic M, Francoeur NJ, Sridhar SH, Smith ML, Khanal S, Britto CJ, Sebra R, Lewis I, Uhlemann AC, Kahl BC, Prince AS, Riquelme SA. 2021. *Staphylococcus aureus* induces an itaconate-dominated immunometabolic response that drives biofilm formation. *Nat Commun* **12**. doi:10.1038/s41467-021-21718-y

Turner NA, Sharma-Kuinkel BK, Maskarinec SA, Eichenberger EM, Shah PP, Carugati M, Holland TL, Fowler VG. 2019. Methicillin-resistant *Staphylococcus aureus*: an overview of basic and clinical research. *Nat Rev Microbiol*. **17**:203-218. doi:10.1038/s41579-018-0147-4

Turner WL, Waller JC, Vanderbeld B, Snedden WA. 2004. Cloning and characterization of two NAD kinases from *Arabidopsis*. Identification of a calmodulin binding isoform.

Plant Physiol **135**:1243–1255. doi:10.1104/pp.104.040428

Van Acker H, Coenye T. 2017. The role of reactive oxygen species in antibiotic-mediated killing of bacteria. *Trends Microbiol*. **25**:456-466. doi:10.1016/j.tim.2016.12.008

Vestergaard M, Frees D, Ingmer H. 2019. Antibiotic resistance and the MRSA problem. *Microbiol Spectr* **7**. doi:10.1128/microbiolspec.GPP3-0057-2018

Vestergaard M, Nøhr-Meldgaard K, Bojer MS, Krogsgård Nielsen C, Meyer RL, Slavetinsky C, Peschel A, Ingmer H. 2017. Inhibition of the ATP synthase eliminates the intrinsic resistance of *Staphylococcus aureus* towards polymyxins. *mBio* **8**. doi:10.1128/MBIO.01114-17

Vestin R. 1937. Enzymic change from codehydrogenase I to codehydrogenase II. *Naturwissenschaften* **25**:667–8.

Von Euler H, Adler E. 1938. Enzymic intertransformation of codehydrogenase I and codehydrogenase II. *Z Physiol Chem* **252**:41–8.

Yin J, Meng Q, Cheng D, Fu J, Luo Q, Liu Y, Yu Z. 2020. Mechanisms of bactericidal action and resistance of polymyxins for Gram-positive bacteria. *Appl Microbiol Biotechnol* **104**:3771–3780. doi:10.1007/s00253-020-10525-y

Zhao C, Shu X, Sun B. 2017. Construction of a gene knockdown system based on catalytically inactive ("dead") Cas9 (dCas9) in *Staphylococcus aureus*. *Appl Environ Microbiol* **83**. doi:10.1128/AEM.00291-17

Zhu Y, Xiong YQ, Sadykov MR, Fey PD, Lei MG, Lee CY, Bayer AS, Somerville GA. 2009. Tricarboxylic acid cycle-dependent attenuation of *Staphylococcus aureus in vivo* virulence by selective inhibition of amino acid transport. *Infect Immun* **77**:4256–4264. doi:10.1128/IAI.00195-09

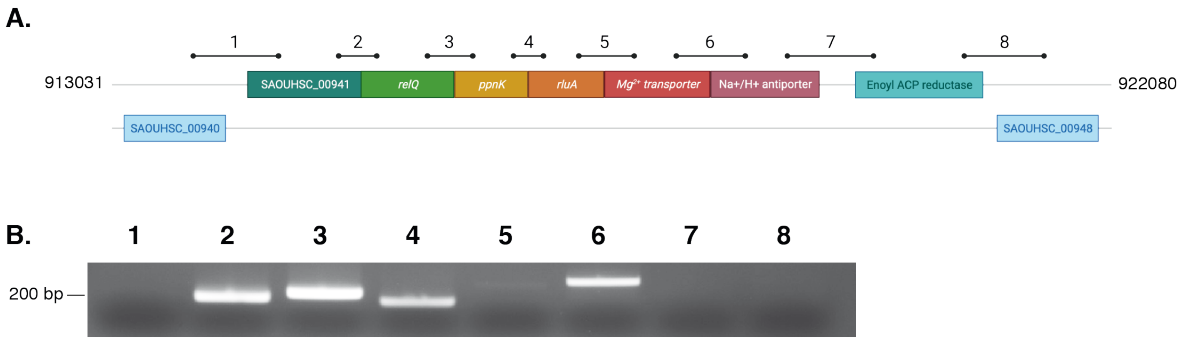

Figure supplement 1 *S. aureus ppnK* gene is part of the *relQ* operon. (A) Genomic region surrounding the *ppnK* gene of *S. aureus* NCTC8325 (sequence NC_007795.1) between nucleotides 913031 and 922080. Bars and numbers represent the regions amplified by RT-PCR. (B) Ethidium bromide staining of DNA in an agarose gel following RT-PCR amplification using total RNA from *S. aureus* NCTC8325 and primers located in regions indicated in (A).

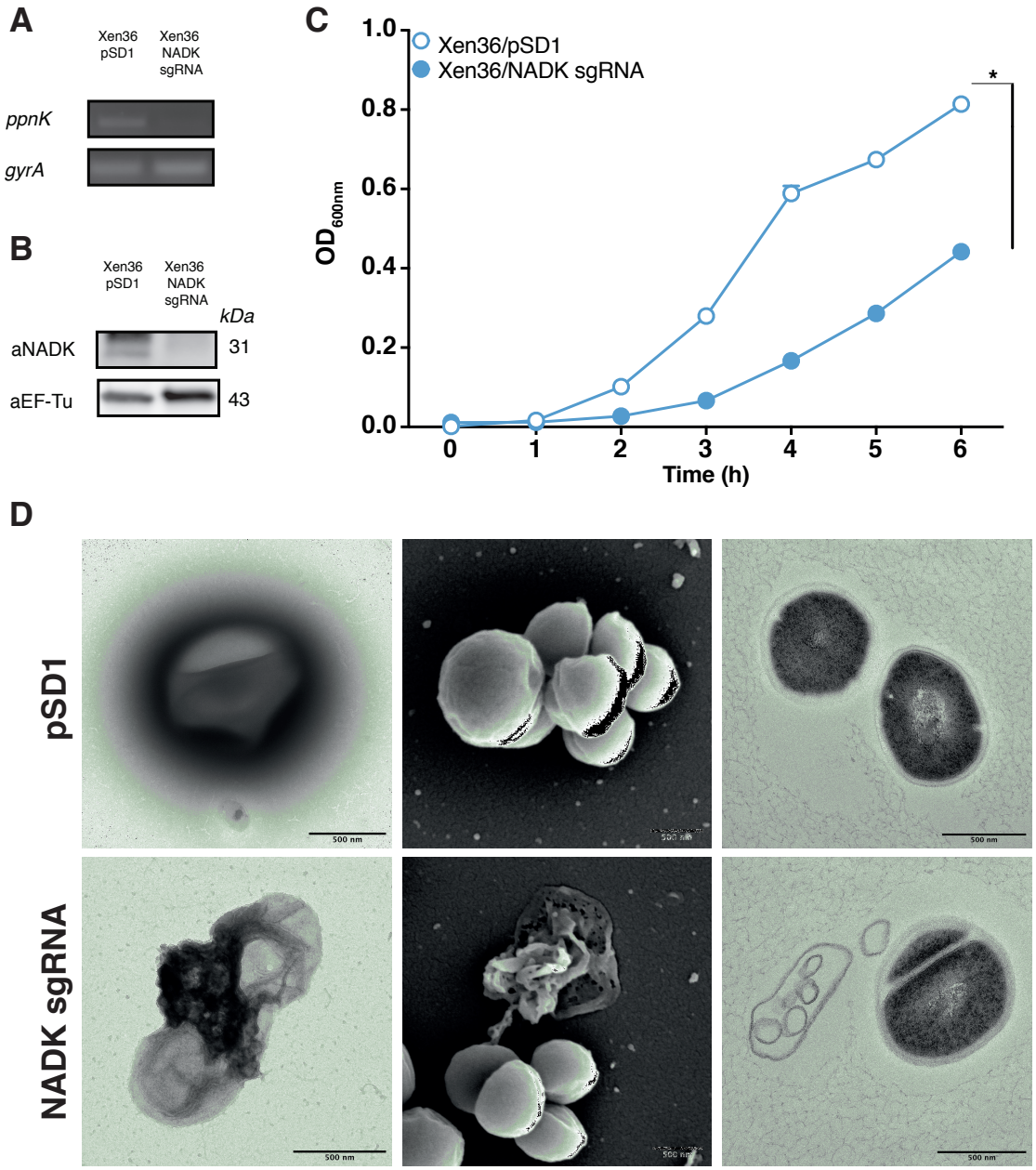

Figure supplement 2 NADK is important for *S. aureus* growth. (A) Total RNA of Xen36/pSD1 and Xen36/NADK sgRNA strains were analyzed by RT-PCR using oligonucleotides in *ppnK* and *gyrA* (control). (B) Bacterial protein extracts of Xen36/pSD1 and Xen36/NADK sgRNA strains were analyzed by immunoblotting using anti-NADK and anti-EF-Tu (control) antibodies. (C) Bacterial growths of Xen36/pSD1 and Xen36/NADK sgRNA strains were monitored for 6 hours at OD_{600nm} in BHI broth at 37°C with ATc induction for *ppnK* knock-down. Data shown are representative of three independent experiments (n=3). Bars indicate the standard error of the means of biological replicates. Comparison of data was performed using a t test (*p<0.05). (D) Negative contrast (left), SEM (central) and TEM (right) images of Xen36/pSD1 (top) and Xen36/NADK sgRNA (bottom) strains after 6 hours of growth. Scale bar: 500 nm.

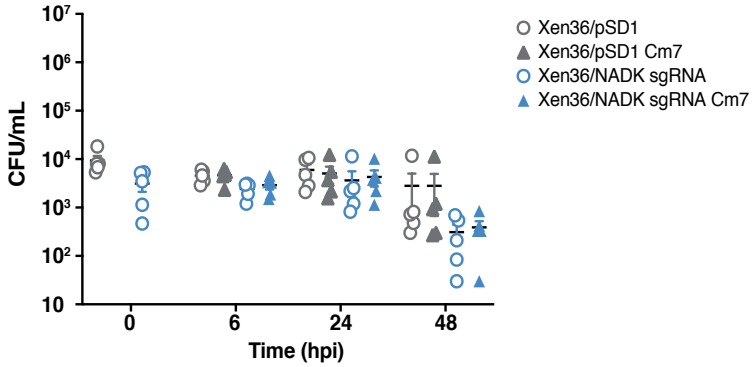

Figure supplement 3 Plasmids are conserved during *S. aureus* infection of zebrafish. The number of Xen36/pSD1 (grey) or Xen36/NADK sgRNA (blue) *S. aureus* was monitored in zebrafish larvae after intravenous injection with 5.10^3 bacteria. For each strain, CFU were determined 6, 24 and 48 hours post-infection by plating fish lysates on BHI (circles) and BHI supplemented with chloramphenicol (triangles) (n=5).